BIDIRECTIONAL Z-SOURCE INVERTER MODELING AND SMITH PREDICTOR STRATEGY FOR MINIMIZING RIGHT HALF ZERO PLAN IN THE VOLTAGE LOOP

Angelo E. Lanzoni[1], Cassiano Rech[2] and Joselito A. Heerdt[1]
[1]Santa Catarina State University - UDESC, Joinville – Santa Catarina, Brazil
[2]Federal University of Santa Maria – UFSM, Santa Maria – Rio Grande do Sul, Brazil
angelo.lanzoni.2012@gmail.com, rech.cassiano@gmail.com ,joselito.heerdt@udesc.br

***Abstract* – This paper shows a different approach to obtain current and voltage models for the Bidirectional Z-Source Inverter, considering the two variables available, which are modulation index and the shoot through duty ratio. Since the shoot through index is the variable that allows to boost the output voltage, the focus is given to use this control variable and the modulation index is kept constant. Moreover, a Smith predictor technic is used to deal with the right half plan zero issue. Simulations results have shown that the model is consistent and the control strategy chosen is advantageous to obtain better dynamic response.**

***Keywords* – Bidirectional Z-Source Inverter, Electrical Vehicle, Modeling, Smith Predictor.**

I. INTRODUCTION

Due to the increasing demand for emissions reduction of vehicles, much effort has been put into research for Electric Vehicles (EVs). As an example, the German government, where major vehicle manufacturers have their head office, has imposed dates for the end of the production of vehicles with internal combustion engines by 2030, and by 2050 there should no longer be such vehicles in circulation.

Mentioned this fact, it is evident the importance of investing efforts in development of EVs. There are two main fields of research when it comes to the EV traction systems: the electric machine that provides torque and speed to the automobile, and the power converter that gives regulated voltage and current to power this machine.

Toward the electric machines, the basic requirements are [1-3]:

- high power density and high torque;
- high speed range;
- high starting torque;
- high efficiency;
- high reliability and robustness;
- low audible noise and low torque ripple;

Several studies have been done about which machine should be ideal for this application [1, 2, 4-6]. There are also studies that developed different types of machines [6-9]. Despite this, those said traditional electrical machine, such as DC machine, Induction Machine (IM), Switched Reluctance Machine (SRM) and Permanent-Magnet Brushless machine are more suitable and used by the manufacturers [1, 2]. However, those currently more appropriate for traction are the Permanent-Magnet Brushless AC machine (PM BLAC) and the IM [2].

With this consideration in mind, the approach about the power converter is towards of those that can operate the IM and the BLAC as well. For the specific case of EVs, the power converter requirements are much more demanding as follow [10]:

- operation in high temperature;
- high mechanical stress;
- reduced weight and volume;
- high proportion between the peak power and the average power.

As in the case for the electrical machines, several power converters have been studied and proposed for EVs [5, 10-15], such as the usual Voltage Source Inverter (VSI), Multilevel Inverters and the promising topology of the Bidirectional Z-Source Inverter (BZSI).

Thus, in this paper, the study of the BZSI will be done concerning modelling and controlling this topology. Plenty of models have been proposed for the ZSI [16-18] However, an important stage is neglected, and only one control parameter is used to represent the converter. By introducing the stage of null vector, it is possible to add equations that characterizes with better accuracy the inverter [18]. Another issue is that the voltage plant has nonminimum phase behavior, making the controller design more difficult. To overcome it, it is proposed the use of a Smith Predictor technic [19-21].

This paper is organized as follows. In section II the relevant consideration for modelling the chosen topology is addressed, as well as its validation via simulation. In section III, the obtained plants are used for the controllers design, and due to the nonminimum phase characteristic, it is proposed the use of Smith Predictor for the voltage loop. In section IV, the simulation results are shown and discussed, with focus on comparing the advantages and disadvantages of using the Smith Predictor. And in section V, a conclusion about the obtained models and proposed loop control is made.

II. BIDIRECTIONAL Z-SOURCE INVERTER MODELING

This section presents the modeling technic used for the BZSI, and its validation via simulation, comparing the Bode diagram of the circuit and the transfer functions obtained.

978-1-5090-6248-5/17/$31.00 ©2017 IEEE

A. Mathematical Converter Analysis

The BZSI uses a *LC* network to have buck-boost capability by using shoot through in its switching logic command. With this specific impedance network, the circuit becomes much more complex than the regular VSI. Besides the usual control variable, the modulation index *M*, this converter has an extra control variable, the shoot through duty cycle D_0. Thereby the BZSI shown in Fig. 1 can control the capacitors voltage in the Z-network and the output voltage at the same time.

For a three-phase power inverter with balanced load, the output power is always constant, thereby, the AC side can be simplified as a DC load without losing generality. Therefore, the circuit can be reduced as it is represented in the Fig. 2.

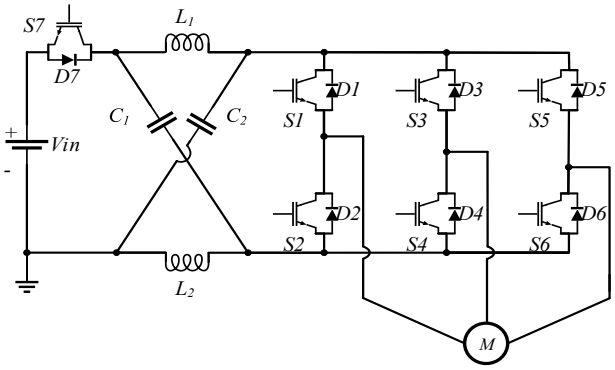

Fig. 1. Bidirectional Z-Source Inverter topology.

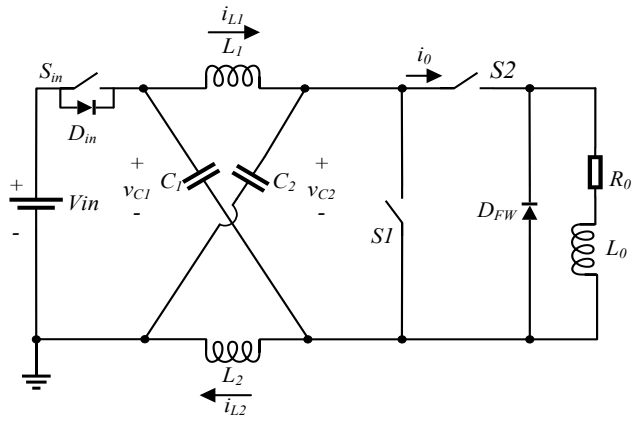

Fig. 2. Simplified circuit for modeling analysis.

Fig. 3 shows the modulation strategy, which consists of three sinusoidal waves with 1/6 of third harmonic, *Va*, *Vb* and *Vc*, each one corresponding the reference for the load voltage. The amplitude of these signals is given by the modulation index. Also, there are two lines *Vp* and *Vn*, that allows the use of shoot-through command and the value is given by the shoot-through duty ratio.

The equivalent circuit has three switches. Switch *S1* is commanded with D_0 index, and switch *S2* is commanded with *M* index. It is emphasized that $D_0 + M \leq 1$. The switch S_{in} is commanded with the complementary of D_0 and allows bidirectional current flow. There is the input diode D_{in} needed for the shoot through stage. There is also a freewheeling diode D_{FW}, and a correspondent *RL* load composed of R_0 and L_0.

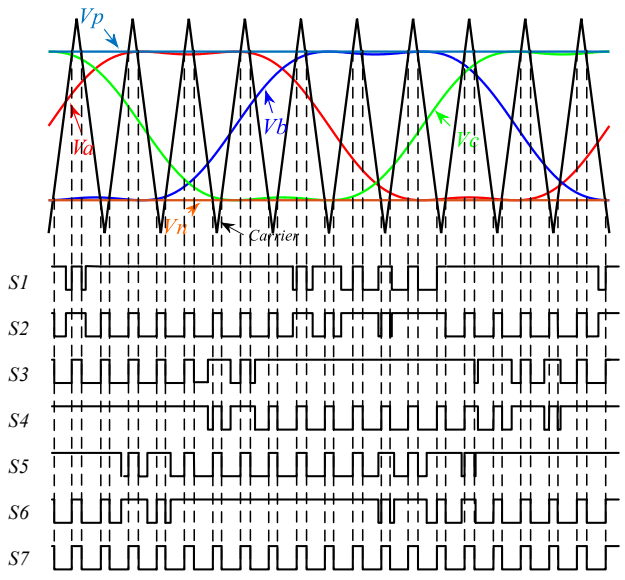

Fig. 3. Maximum constant boost with third harmonic modulation.

Such components correspond to the AC part that has been simplified. The resistance R_0 can be found based on the power balance [18]:

$$R_0 = \frac{8|Z|}{3\cos(\varphi)} \tag{1}$$

where *Z* is the impedance of the three-phase load, and cos(φ) is the load power factor. The inductance L_0 is calculated such that the constant time of the DC load is the same of the AC load:

$$\frac{R_0}{L_0} = \frac{R_{ac}}{L_{ac}} \tag{2}$$

where R_{ac} and L_{ac} are the resistance and inductance of the three-phase load, respectively.

Assuming that the Z-network is symmetrical, it means that the capacitors are identical, $C_1 = C_2 = C$, and the same is valid for the inductors, $L_1 = L_2 = L$. Therefore, the currents in the inductors are the same, $i_{L1} = i_{L2} = i_L$, and the capacitors voltage are the same as well, $v_{C1} = v_{C2} = v_C$.

With those assumptions, the variables to be analyzed are:

- The inductor current i_L;
- The capacitor voltage v_C;
- The output current of Z-network i_0.

Considering the simplified circuit, there are three operation stages. The first one happens when the switch *S1* is turned on the switch *S2* is off. The switch S_{in} is off, and due to the capacitors being associated in series in this stage, the voltage is higher than the input voltage source V_{in}, so the diode D_{in} is off, isolating the source from the impedance network. This is the corresponding shoot through state. In this stage, the capacitors provide energy for the inductors and the load current flows through the freewheeling diode. The time duration of this stage is $D_0.T$, where *T* is the switching period. The equations for this stage are:

$$L\frac{di_L(t)}{dt} = v_C(t)$$
$$C\frac{dv_C(t)}{dt} = -i_L(t) \quad (3)$$
$$L_0\frac{di_0(t)}{dt} = -R_0 i_0(t)$$

The second stage happens when *S1* and *S2* are off. The switch S_{in} is on. This stage is correspondent to the traditional stage of null vector. It is important to emphasize that this stage is commonly neglected in other works, loosing accuracy. During this stage, the capacitors are charged by the inductor, and the load current goes through the freewheeling diode. The time duration of this stage is $(1 - D_0 - M).T$. The equations for this stage are:

$$L\frac{di_L(t)}{dt} = -v_C(t) + v_{in}(t)$$
$$C\frac{dv_C(t)}{dt} = i_L(t) \quad (4)$$
$$L_0\frac{di_0(t)}{dt} = -R_0 i_0(t)$$

The third stage occurs when *S1* is off and *S2* and S_{in} are on, thus the current flow depends if it is on traction or regeneration mode. This is the stage corresponding to those with active vectors, when there is energy flow from the input source to the load or the opposite as well. The time duration of this stage is $M.T$. The equations for this stage are:

$$L\frac{di_L(t)}{dt} = -v_C(t) + v_{in}(t)$$
$$C\frac{dv_C(t)}{dt} = i_L(t) - i_0(t) \quad (5)$$
$$L_0\frac{di_0(t)}{dt} = 2v_C(t) - v_{in}(t) - R_0 i_0(t)$$

The transfer functions obtained in this paper are based on the averaging technic. It consists in calculating the average value in every switching period, posteriorly it is inserted a disturbance to the quiescent value. Lastly, it is applied the Laplace Transform. In this work, the effort was done towards the shoot through duty cycle variable, since it is the key to achieve the buck-boost characteristic of this topology. After some algebraic rearrangement, the models achieved are given by:

$$G_{vC\_d0} = \frac{V_C(s)}{d_0(s)} = \frac{s^2 n_{v2} + s n_{v1} + n_{v0}}{s^3 d_3 + s^2 d_2 + s d_1 + d_0} \quad (6)$$

$$G_{iL\_d0} = \frac{I_L(s)}{d_0(s)} = \frac{s^2 n_{i2} + s n_{i1} + n_{i0}}{s^3 d_3 + s^2 d_2 + s d_1 + d_0} \quad (7)$$

where $n_{v2} = -2L_0 L I_L$, $n_{v1} = L_0 V_{in} - 2LR_0 I_L$, $n_{v0} = R_0 V_{in}$, $n_{i2} = CL_0(2V_C - V_{in})$ $n_{i1} = CR_0(2V_C - V_{in}) + 2I_L L_0(1 - 2D_0)$ $n_{i0} = 2M^2(2V_C - V_{in}) + 2I_L L_0(1 - 2D_0)$, $d_3 = CLL_0$, $d_2 = CLR_0$, $d_1 = 2M^2 L + L_0(1 - 2D_0)^2$, and $d_0 = R_0(1 - 2D_0)^2$.

B. Models Validation

In order to validate the models, a comparison of the Bode diagrams for the voltage and current plants with the corresponding Bode diagrams obtained with the simplified circuit shown in Fig. 2 was done.

The parameters used for simulation are given in TABLE I:

TABLE I
Circuit Simulation Parameters

Parameters	Value	Unit
V_{in}	300	*V*
V_C	550	*V*
I_L	2,579	*A*
M	0,6603	-
D_0	0,3125	-
L	15,4	*mH*
C	2,2	*μF*
R_0	360,586	Ω
L_0	667,63	*mH*

Fig. 4 and Fig. 5 show the voltage and current models respectively. It is noted that the Bode diagram of the transfer functions match with the simulated circuit in practically all range of frequency, thus validating the models.

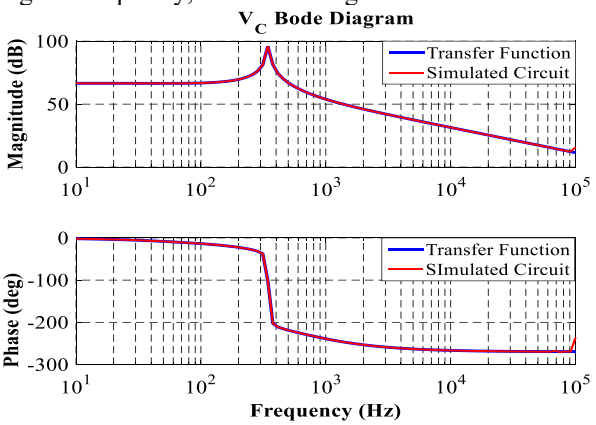

Fig. 4. Bode diagram of voltage plant and simplified circuit comparison.

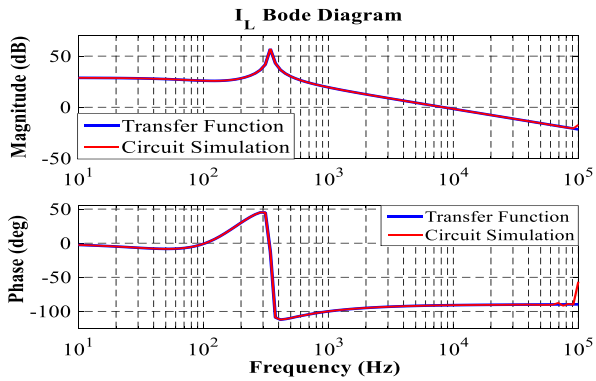

Fig. 5. Bode diagram of current plant and simplified circuit comparison.

With these two models, the control loop adopted [16] is shown in Fig. 6, where there is an inner loop composed of the current plant $G_{iL\_d0}(s)$ and its corresponding controller $C_{iL}(s)$. The Pulse Width Modulation (PWM) characteristic is also

represented as well as the current sensor $H_i(s)$. The outer loop is composed of the voltage plant $G_{vC\_d0}(s)$, its sensor $H_v(s)$, and the controller $C_{vC}(s)$. The voltage loop is complex to control, because the plant has a Right-Half Plane Zero (RHPZ). To overcome the limitation that is imposed by this zero, the next section will discuss the use of a Smith predictor control technic. Whereas D_0 was chosen to be control variable, M was kept constant in this work, although it can also be controlled as well in a separated loop using the same approach and respecting the limitation of $D_0 + M \leq 1$.

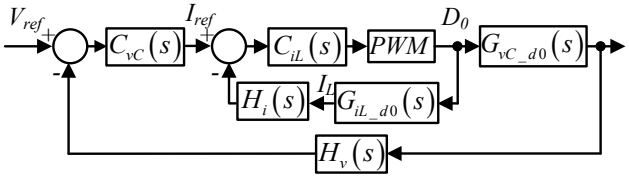

Fig. 6. Dual loop control configuration.

III. SMITH PREDICTOR CONTROL STRATEGY FOR NONMINIMUM PHASE VOLTAGE PLANT

This section presents the Smith Predictor control technic used for the BZSI voltage loop, and it is also shown a voltage controller with Proportional Integral (PI) action for further simulation comparison. As the current loop does not present this nonminimum phase characteristic, for both cases, the controller design will be the same.

A. Smith Predictor

As seem previously, the transfer function of capacitor voltage by shoot through duty ratio has a zero located at the right-half complex plan. This zero makes the controller design more complex to achieve the stabilization criteria [22]. To overcome this difficulty and minimize the effect of RHPZ, in this paper is discussed the Smith Predictor method for the voltage loop.

The structure of the Smith Predictor can be divided into two parts. One with the controller and the other with the predictor structure. The controller $C(s)$ is usually a Proportional Integrative Derivative (PID), but can also be a higher-order. The predictor is composed of a model of the plant without RHPZ $G_n(s)$ and a part to cancel the RHPZ ($\lambda.s$). The plant is factored in $G_n(s)$ and ($1 - \eta.s$) that correspond to the RHPZ.

The feedback of the controller is:

$$G'(s) = G_n(s)\lambda.s \tag{8}$$

The goal is to choose λ which makes the controller have a response equivalent to a process without RHPZ. Defining the feedback signal of the controller as:

$$Y'(s) = G'(s)U(s) \tag{9}$$

Therefore,

$$E_f(s) = R(s) - Y(s) - Y'(s) \tag{10}$$

$$E_f(s) = R(s) - \left[G(s) + G'(s)\right]U(s) \tag{11}$$

and defining

$$\begin{aligned} G^*(s) &= G(s) + G'(s) \\ Y^*(s) &= G^*(s)U(s) \end{aligned} \tag{12}$$

The fixed error $E_f(s)$ becomes

$$E_f(s) = R(s) - Y^*(s) \tag{13}$$

From the point of view of the controller $C(s)$, the process generates the signal $Y^*(s)$, with

$$\begin{aligned} G^*(s) &= G_n(s)(1 - \eta.s) + G_n(s)(\lambda.s) \\ G^*(s) &= G_n(s)\left[1 + (\lambda - \eta).s\right] \end{aligned} \tag{14}$$

Choosing λ that $\lambda \geq \eta$, the transfer function of the process does not appear to have RHPZ. To minimize the mean square error, $\lambda = 2.\eta$ is the optimum value [22]. The final block diagram is shown in Fig. 7.

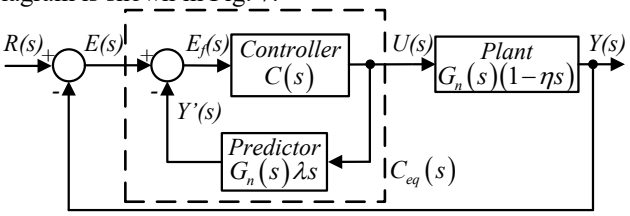

Fig. 7. Smith Predictor control loop configuration.

B. Controllers Design

The inner current loop control is easier to design. It has been done by poles-zeros cancellation. The gain crossover frequency was chosen to be 1kHz, since the switching frequency was chosen to be 10kHz. The phase margin should be at least 45° to guarantee stability. However, the voltage loop needs a smaller gain crossover frequency, in such way that the time response of both controllers does not conflict due to the dual loop configuration chosen. Also, to achieve the stability criteria, the cutting frequency needs to be even smaller, due to the presence of the RHZP, for a PI control strategy.

To compare the advantages of using Smith Predictor in the outer loop, it was designed a PI controller by poles-zeros cancellation, with an extra pole to filter high frequency noise, for the voltage loop. The cutting frequency was chosen to be 100Hz, since the switching frequency of the current loop is 1kHz, in other words, one decade of difference. The phase margin should be at least 45° to guarantee stability. Afterwards it will be shown how the circuit will respond with the regular loop control and with the Smith Predictor loop rearranging. In sequence, it is shown the Bode Diagram for the current control in Fig. 8, the Bode diagram for both, voltage loop without and with Smith Predictor in Fig. 9.

The controller designed and the Smith Predictor $P(s)$ are shown below:

$$C_{iL}(s) = 84.5\frac{0.0022s + 1}{s\left(1.6\times10^{-5}s + 1\right)} \tag{15}$$

$$C_{vC}(s) = 1164\frac{0.0014s + 1}{s\left(0.00016s + 1\right)} \tag{16}$$

$$C_{vCP}(s) = 1500\frac{0.00039s + 1}{s\left(0.00016s + 1\right)} \tag{17}$$

$$P(s) = \frac{3.885\times10^{11}s^3 + 3.063\times10^{14}s^2 + 6.908\times10^{16}s}{6.304\times10^{4}s^5 + 3.694\times10^{8}s^4 + 1.167\times10^{12}s^3 + 7.442\times10^{14}s^2 + 1.296\times10^{17}s} \tag{18}$$

where $C_{vCP}(s)$ is the controller designed for the case with the predictor on the voltage loop.

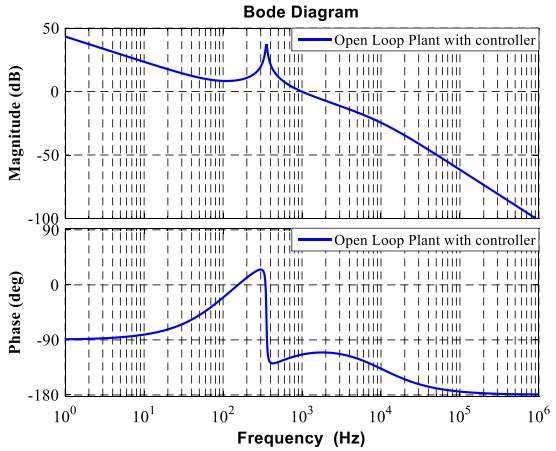

Fig. 8. Bode diagram for the current open loop transfer function with controller.

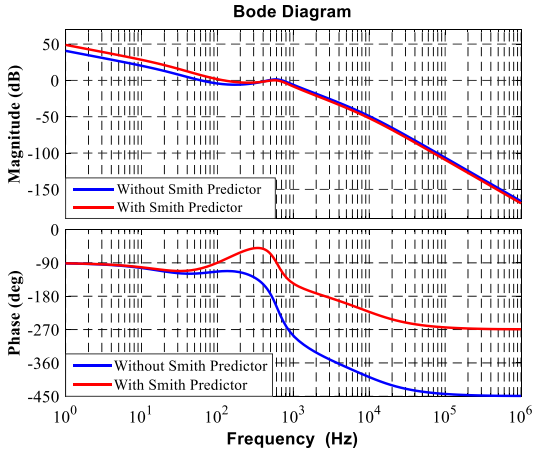

Fig. 9. Bode diagrams for the voltage open loop transfer function with controller without and with Smith Predictor.

IV. SIMULATION RESULTS AND DISCUSSION

This section presents the simulation results for a 50% to 100% and back to 50% load step for both cases. The circuit utilized for this part was the usual BZSI, not the simplified version. Fig. 10 and Fig. 11 shows the voltage at the capacitor and the current at the inductor, respectively, for both voltage loop controllers strategies. The use of Smith Predictor to minimize the RHPZ makes the response faster and reduce the low frequency ripple in the transient response caused by the zero presence.

This advantage happens since the controller is designed for a plant that doesn't present a zero in the right side of the imaginary plan. It allows to design controllers with higher gains, resulting in faster settling time. One notable disadvantage is the complexity add in the voltage loop with the predictor presence. It also causes more computational demand, although it is not so evident when is considered the fast DPSs and FPGAs available.

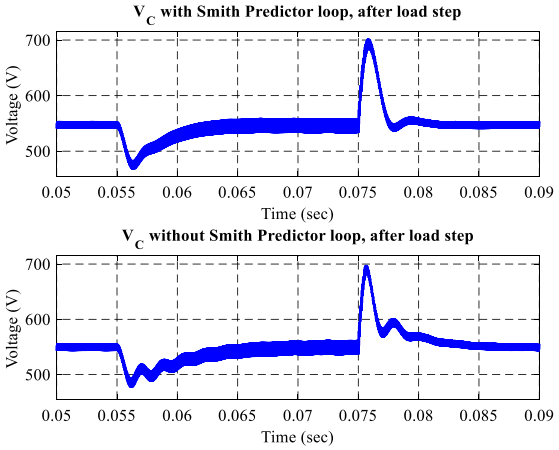

Fig. 10. Capacitor voltages and inductor currents after load step for different control strategies comparison.

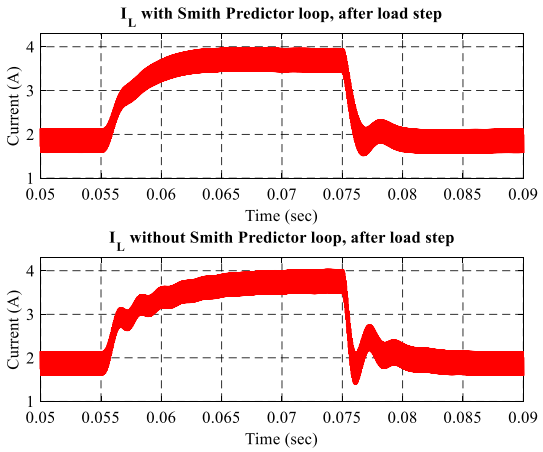

Fig. 11. Inductor currents after load step for different control strategies comparison.

V. CONCLUSIONS

A different analysis for modeling the BZSI has been done. It included a stage that is commonly neglected, which affects the behavior representation of the circuit. When the stage of null load voltage is included, it is possible to use two control variables to represent the models, the modulation index M and the shoot through index D_0.

The work on this paper has focused into the shoot-through index, since it is the key to have the buck-boost single stage characteristic for this converter topology. Other issue is that the voltage plant has RHZP, making the controller design difficult. To overcome it, it has been done an approach that includes the Smith Predictor into the voltage loop. This consideration has made the loop more complex, but the results of better dynamic behavior and fast response compensate the effort.

ACKNOLEDGEMENTS

The authors thank UDESC, FAPESC, CAPES and FITEJ for the financial support of this work.

REFERENCES

[1] K. T. Chau, C. C. Chan, and L. Chunhua, "Overview of Permanent-Magnet Brushless Drives for Electric and Hybrid Electric Vehicles," *Industrial Electronics, IEEE Transactions on,* vol. 55, pp. 2246-2257, 2008.

[2] X. Wei, Z. Jianguo, G. Youguang, W. Shuhong, W. Yi, and S. Zhanghai, "Survey on electrical machines in electrical vehicles," in *Applied Superconductivity and Electromagnetic Devices, 2009. ASEMD 2009. International Conference on*, 2009, pp. 167-170.

[3] Z. Q. Zhu and D. Howe, "Electrical Machines and Drives for Electric, Hybrid, and Fuel Cell Vehicles," *Proceedings of the IEEE,* vol. 95, pp. 746-765, 2007.

[4] J. B. Bartolo and C. Gerada, "The electromagnetic design of a high speed, 45kW, switched reluctance machine having a novel rotor geometry for aerospace application," in *Electrical Machines (ICEM), 2014 International Conference on*, 2014, pp. 2513-2519.

[5] K. T. Chau, *Electric Vehicle Machines and Drives: Design, Analysis and Application*: Wiley, 2015.

[6] A. Walker, M. Galea, C. Gerada, A. Mebarki, and D. Gerada, "A topology selection consideration of electrical machines for traction applications: towards the FreedomCar 2020 targets," in *Ecological Vehicles and Renewable Energies (EVER), 2015 Tenth International Conference on*, 2015, pp. 1-10.

[7] P. Giangrande, D. Ronchetto, G. Pellegrino, F. Cupertino, C. Gerada, and M. Sumner, "Hybrid sensorless control of axial flux permanent magnet motor drives, including zero speed," in *Power Electronics and Applications (EPE 2011), Proceedings of the 2011-14th European Conference on*, 2011, pp. 1-8.

[8] E. Padurariu, L. E. Somesan, l. A. Viorel, and L. Szabo, "Large power permanent magnet transverse flux motor, steady-state and dynamic behavior," in *ELEKTRO, 2012*, 2012, pp. 221-224.

[9] Verse, x, C. le, Z. De Greve, F. Vallee, R. Hanuise*, et al.*, "Analytical design of an axial flux permanent magnet in-wheel synchronous motor for electric vehicle," in *Power Electronics and Applications, 2009. EPE '09. 13th European Conference on*, 2009, pp. 1-9.

[10] S. Miaosen and P. Fang Zheng, "Converter systems for hybrid electric vehicles," in *Electrical Machines and Systems, 2007. ICEMS. International Conference on*, 2007, pp. 2004-2010.

[11] J. Bum-Seung, L. Won-kyo, K. Tae-Jin, K. Dae-Wook, and H. Dong-seok, "A study on the multi-carrier PWM methods for voltage balancing of flying capacitor in the flying capacitor multi-level inverter," in *Industrial Electronics Society, 2005. IECON 2005. 31st Annual Conference of IEEE*, 2005, p. 6 pp.

[12] O. Ellabban, J. V. Mierlo, and P. Lataire, "Control of a bidirectional Z-Source Inverter for hybrid electric vehicles in motoring, regenerative braking and grid interface operations," in *Electric Power and Energy Conference (EPEC), 2010 IEEE*, 2010, pp. 1-6.

[13] P. Lezana and G. Ortiz, "Extended Operation of Cascade Multicell Converters Under Fault Condition," *Industrial Electronics, IEEE Transactions on,* vol. 56, pp. 2697-2703, 2009.

[14] B. Sarrazin, N. Rouger, J. P. Ferrieux, and Y. Avenas, "Benefits of cascaded inverters for electrical vehicles' drive-trains," in *Energy Conversion Congress and Exposition (ECCE), 2011 IEEE*, 2011, pp. 1441-1448.

[15] P. G. Song, E. Y. Guan, L. Zhao, and S. P. Liu, "Hybrid Electric Vehicles with Multilevel Cascaded Converter using Genetic Algorithm," in *Industrial Electronics and Applications, 2006 1ST IEEE Conference on*, 2006, pp. 1-6.

[16] O. Ellabban, J. V. Mierlo, and P. Lataire, "Voltage mode and current mode control for a 30 kW high-performance Z-source Inverter," in *Electrical Power & Energy Conference (EPEC), 2009 IEEE*, 2009, pp. 1-6.

[17] J. Liu, J. Hu, and L. Xu, "Dynamic Modeling and Analysis of Z Source Converter-Derivation of AC Small Signal Model and Design-Oriented Analysis," *IEEE Transactions on Power Electronics,* vol. 22, pp. 1786-1796, 2007.

[18] M. Shen, Q. Tang, and F. Z. Peng, "Modeling and Controller Design of the Z-Source Inverter with Inductive Load," in *2007 IEEE Power Electronics Specialists Conference*, 2007, pp. 1804-1809.

[19] S. Bag, T. Roy, S. Mukhopadhyay, S. Samanta, and R. Sheehan, "Boost converter control using Smith Predictor technique to minimize the effect of Right Half Plane zero," in *2013 IEEE International Conference on Control Applications (CCA)*, 2013, pp. 983-988.

[20] F. A. Himmelstoss, J. W. Kolar, and F. C. Zach, "Analysis of a Smith-predictor-based-control concept eliminating the right-half plane zero of continuous mode boost and buck-boost DC/DC converters," in *Industrial Electronics, Control and Instrumentation, 1991. Proceedings. IECON '91., 1991 International Conference on*, 1991, pp. 423-428 vol.1.

[21] D. Mukherjee and D. Ghose, "Smith predictor based control strategies for nonminimum phase plants," in *2013 IEEE International Conference on Control Applications (CCA)*, 2013, pp. 948-953.

[22] J. E. Normey-Rico, *Control of Dead-time Processes*: Springer London, 2009.